Appl. Phys. A 81, 759–762 (2005)
DOI: 10.1007/s00339-004-2996-0

Applied Physics A
Materials Science & Processing

J.D. YE✉
S.L. GU
F. QIN
S.M. ZHU
S.M. LIU
X. ZHOU
W. LIU
L.Q. HU
R. ZHANG
Y. SHI
Y.D. ZHENG

Correlation between green luminescence and morphology evolution of ZnO films

Department of Physics, Nanjing University, Nanjing 210093, P.R. China

Received: 5 April 2004/Accepted: 20 July 2004
Published online: 31 August 2004 •

ABSTRACT Photoluminescence and atomic force microscopy have been used to characterize ZnO thin films grown by metal-organic chemical vapor deposition (MOCVD) at varied growth pressures. The surface morphology with different grain structures has strong influence on the green photoluminescence of ZnO. When large discrete islands or structureless overgrowth cover the rough surface, broad green emissions around 500 nm go beyond the ultraviolet (UV) emission band; whereas, when the surface is packed closely with small grains, only weak green emission is observed with a red-shift to 528 nm. This variation of green emissions is ascribed to changes in the charge states of oxygen vacancies, which is strongly dependent on the surface morphology and grain structures. Based on the grain boundary defect model, two possible recombination processes for the green emission are proposed and discussed in detail.

PACS 68.55.Jk; 78.55.Et; 81.05.Dz

1 Introduction

Recently, wide band gap material zinc oxide (ZnO) besides GaN is attracting much attention as a promising candidate for opto-electric applications in UV and green regions [1]. Generally, an intense and board emission in the green range (2.2–2.5 eV) has been observed, especially evident in the nano-size particles or the polycrystalline ZnO [2, 3]. The nature of green emission has been the subject of much research. This emission was thought to be associated with native defects in the undoped ZnO such as interstitial zinc [4], oxygen vacancies [2, 3, 5, 6] and interstitial oxygen [5, 7] or zinc vacancies [8, 9]. During the past years, oxygen vacancies have been assumed to be the most likely candidates for the recombination centers involved in the green luminescence, which has been identified recently by F.H. Leiter et al. [10]. However, the green luminescence is sensitive to the defect chemistry. A. van Dijken et al. [3, 11] proposed that the visible emission is due to the recombination of an electron from the conduction band with a deep electron-trapping center of V_O^{++}, and alternatively, K. Vanheusden et al. [2] give a conclusion that the recombination of isolated V_O^+ center with photoexcited holes are responsible for the green emission.

According to the well-known grain boundary defect model proposed by Gupta [12], the charge states of the defects are strongly dependent on the surface morphology and grain structure [2, 12, 13]. Grain boundary in semiconductors leads to potential fluctuations, and band bending effect plays an important role in the changes of defect chemistry. The electronic structure of ZnO grain boundaries has been characterized by positron annihilation spectroscopy [12] and the spatially resolved electron energy loss spectroscopy [14]. To date, few studies have been devoted to the influence of the surface morphology on the photoluminescence properties of ZnO, although the similar results on CdTe [15] and GaN [16] have been reported. In this study, the correlation of surface morphology and green emissions are studied and the possible transition processes for green emissions are proposed on the basis of the grain boundary defect model.

2 Experiments

ZnO films have been deposited on (0001) sapphire substrates by our homemade low-pressure metal–organic chemical vapor deposition (LP-MOCVD) system. Details of the growth procedure were described elsewhere [17]. Diethylzinc (DEZn) and 5N-purity O_2 were used as zinc precursor and oxygenic source, respectively. 5N-purity Ar gas was employed as the carrier gas of DEZn, and also as the buffer gas to prevent the source gases upstream. The ratio of VI/II mass flow rate is fixed at 220 to keep the stoichiometric composition. Series samples were grown at 400 °C for 30 min via varying the growth pressure from 14 pa to 240 pa. The growth rate increased with the pressure, and the thicknesses were 180, 350 and 560 nm for samples grown at 14, 60 and 240 pa, respectively. The surface morphology was characterized by a DI Nanoscope IIIa atomic force microscope (AFM) in contacting mode. Photoluminescence (PL) spectra were recorded by using He-Cd (325 nm) laser as the excitation source. Hall measurements were taken in the Van der Pauw configuration with indium ohmic electrodes. All the measurements were carried out at room temperature.

✉ Fax: +86-25/368-5485, E-mail: hmdl@netra.nju.edu.cn

3 Results and discussions

The surface morphology and the grain growth are strongly dependent on the growth pressure. Three different surface patterns and grain structures are presented in Fig. 1. All AFM pictures are scanned over a scale of $1 \times 1\ \mu m^2$ and the cross-sectional profiles are available for better viewing. The morphology of film grown at 14 pa is dominated by a typical "discrete island"-like structures with three-dimensional growth features of large grains and rough surface (Fig. 1a). Due to the high interfacial energy associated with the ZnO on sapphire and the high gas velocity, the nucleation density would be low during the initial growth stage, and subsequently, the adatoms preferred to combine with the nucleating sites, promoting the combined effect of crystallite size. It is believed that the growth of nuclei leads to discrete island formation and a rough surface, which undergo a typical 3D growth mode. Grown at a moderate pressure of 60 pa, the film structure appears uniform all over the substrate surface, and the columnar grains are well- aligned and close-packed (Fig. 1b). These features are expected to be formed in the column-like growth mode. According to the Walton–Rhodin atomistic theory of nucleation [18], the nucleation rate is proportional to the growth rate. In the early growth stage, nuclei with high density are uniformly distributed on the substrate surface due to the high growth rate. As the grains reach the critical size of nucleation, it will start to grow in size and a well-ordered columnar structure is advanced along the (0002) crystallographic direction. This change in growth mode results in a substantial reduction of surface roughness; however, the grain sizes are limited due to the low surface mobility of adatoms. As the pressure up to 240 pa, a quasi-2D flat continuous film is produced due to the high nucleating density and high growth rate [19]. However, the gas-phase pre-reaction above deposition surface would come forth at high pressure; thus, irregular-shaped structureless overgrowths are highly advanced, causing the surface rough again. Thus, a moderate pressure is essential for the improvement of the surface morphology.

Photoluminescence spectra of samples were shown in Fig. 2, which shows a strong dependence on the surface morphology and grain structures. For all samples, two emission bands are observed. One is a relatively narrow and pronounced emission band in the UV range due to the annihilation of free excitons at room temperature [20], while the other is a broad asymmetric emission band in the green range. Especially for the smooth surface covered by well-ordered grains, the UV emission is dominant with a narrow peak width of 140 meV, indicative of good optical property. It is understandable that the intrinsic defects are reduced within the well-ordered grains, enhancing the luminous efficiency of the UV band. Similar phenomena are observed for GaN films by M. Godlewski et al. [16] who demonstrate that the "edge" emission for the well-resolved grain is more intense than that for the structureless overgrowth.

These spectra all show an asymmetric broad band in the green, but their intensities and positions differed from each other. For better interpreting, these broad bands are Gaussian divided into two bands and assigned as B1 and B2 (Fig. 3) whose positions have a slight change with the sample due to the variations in the local environments of the defect centers in different samples [2]. The ratios of integrated intensities (B1/B2) have different values of 1.26, 0.58 and 7.85 for samples grown at 14, 60 and 240 pa, respectively. It implies that the defect centers for producing the two PL bands are different and compete with each other.

In general, two possible mechanisms for the green emission are considered: (1) recombination of a shallowly trapped (delocalized) electron with a deeply trapped hole, or (2) recombination of a shallowly trapped hole with a deeply trapped electron. Due to the low formation enthalpy, oxygen vacancies are abundant in the crystal as donors [21] and identified as the origin of green emission in the undoped ZnO [10]. However, oxygen vacancies in ZnO often occur in three different charge states: the V_O^x state which has captured two electrons and is neutral relative to the lattice, the single ionized V_O^+ state, and the V_O^{++} state which is doubly positively charged with respect to the lattice. With respect to the nature of trap centers involved in the green emission process, the defect chemistry should be taken into account.

The band-bending effect at the grain boundary plays an important role in the variation of defect chemistry. In semi-

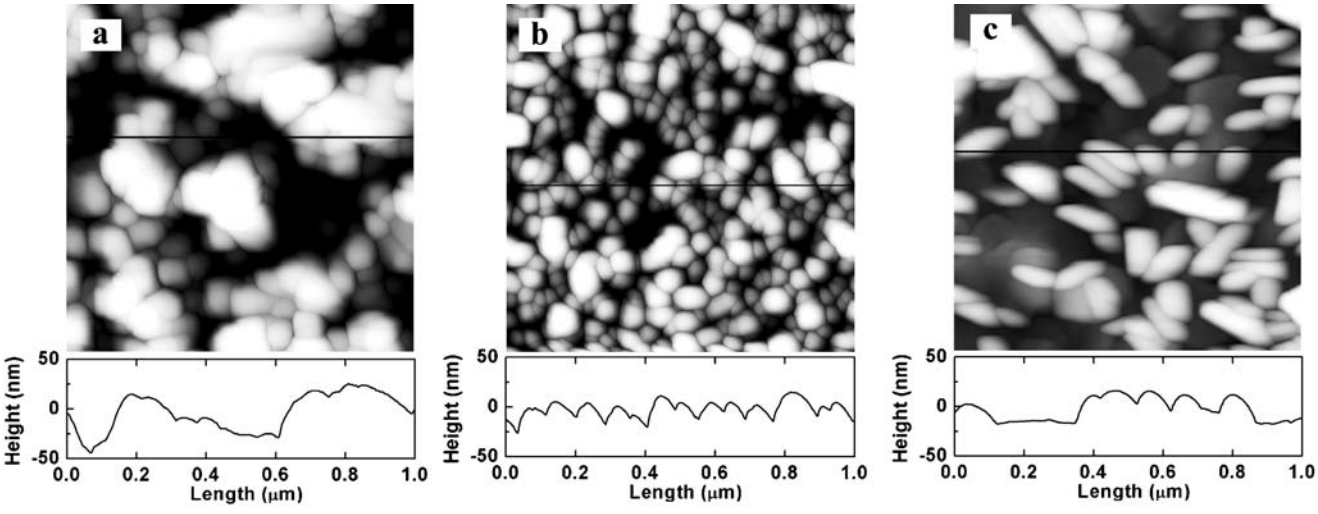

FIGURE 1 AFM images (1 μm × 1 μm) and the cross-sectional profiles for the ZnO films deposited at different pressures: 14 pa **a**, 60 pa **b** and 240 pa **c**

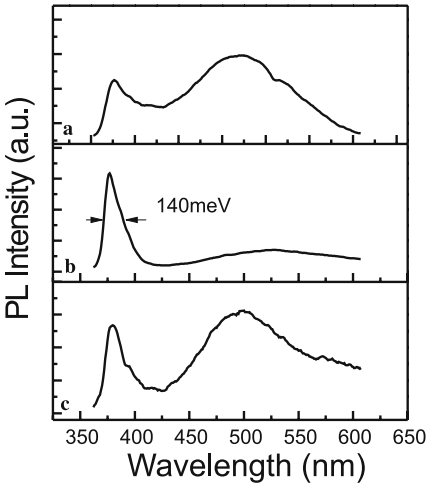

FIGURE 2 Photoluminescence spectra measured at room temperature for the ZnO films deposited at different pressures: 14 pa (**a**), 60 pa (**b**) and 240 pa (**c**)

conductors, grain boundary potential barrier are formed when the grain boundary has a lower chemical potential for majority carriers than the grains. Seager and Castner [22] have constructed the theory of grain-boundary barrier formation and the depletion effect for the polycrystalline semiconductors and good agreements with the experiments were observed in polycrystalline silicon. Moreover, an atomic defect model was proposed for the double Schottky barrier at the grain boundary, assuming donor-like positively charged defects in the depletion layer [12]. Figure 4 shows the energy diagram describing the defect distribution in two semi-infinite grains and one grain boundary. Band bending will create an electron depletion region where the Fermi level passes below the V_O^+/V_O^{++} level, most of oxygen vacancies will be in the diamagnetic V_O^{++} state, while in the bulk region of grains, the majority defects are expected to be in their paramagnetic V_O^+ states. These positively charged states are compensated by a layer of negatively charged ions (such as O^{2-} ions) at the grain boundary interface. However, to what degree band bending impact on the defect chemistry is to a large extent determined by the ratio of the depletion width to the actual grain size. An expression for the depletion width d can be obtained by equating the amount of positive charge around a grain-boundary to the one-dimensional Poisson's equation [22], $d = \left(2\varepsilon_r\varepsilon_0\Phi_B/e^2N_d\right)^{\frac{1}{2}}$, where Φ_B is the height of potential barrier, N_d is the donor concentration, ε_r and ε_0 are the dielectric constant and a relative dielectric permittivity, respectively. In order to estimate the depletion width, the carrier concentrations of films are measured by Hall experiments. The carrier concentrations are $1.63 \times 10^{18}\,cm^{-3}$, $3.25 \times 10^{17}\,cm^{-3}$ and $2.85 \times 10^{18}\,cm^{-3}$, and the depletion widths d are estimated to be 7, 18 and 5 nm for samples grown at 14, 60 and 240 pa, respectively, assuming that N_d is roughly equal to the measured carrier concentration and Φ_B satisfies the relationship with N_d (Fig. 14 in [23]). When $2d$ comparable to the grain size, more than one-half of grains are actually depleted and consequently, the majority defects are of V_O^{++} state, whereas, the depletion region cover a small fraction of the total volume for the larger-grained sample, namely, more oxygen vacancies are of V_O^+ state.

Based on the analysis of defect chemistry above, we now discuss the correlation between the green emissions and the surface morphology. As the surface morphology is dominated by three-dimensional large-grained islands, the intensity of B1 band ($\sim$ 500 nm) overpasses that of B2 band (555 nm). As estimated above, the small depletion width of 7 nm only represents a few percent of the total volume for large grains, and consequently, the majority of oxygen vacancies are of V_O^+ state. This suggests that B1 band is mainly originated from the recombination of V_O^+ center. In fact, V_O^+ can trap a photoexcited electron easily though a non-recombination step [3] to

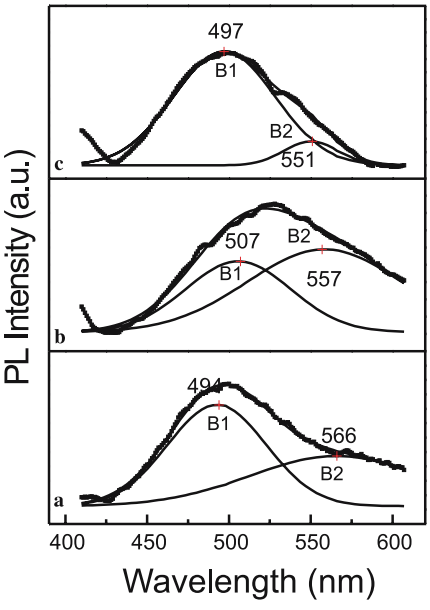

FIGURE 3 Green photoluminescence of the ZnO films at room temperature, Each of spectra is Gaussian divided into two bands, assigned as B1 and B2

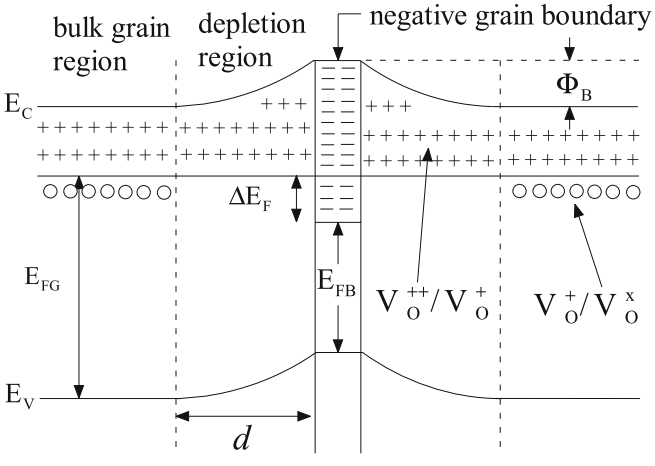

FIGURE 4 Atomic defect model on the basis of a double Schottky barrier describing the distribution of defects in two-semi-infinite grains and one grain boundary, where E_V is the valance band, E_C is the conduction band, E_{FG} is the Fermi level in grains, E_{FB} is the Fermi level in the grain boundary region, ΔE_F is the difference between two regions, Φ_B is the height of potential barrier, d is the width of the depletion layer, and open circles represent neutral states

form the neutral V_O^x center, which is instable at room temperature. Then, a radiative recombination of this center with the photoexcited holes in the valance band takes place effectively, yielding photons with energy of ∼ 2.5 eV. In the case of sample grown at 240 pa, due to the reduction of depletion width and the large coverage of the continuous flat layer under overgrowth, band bending can be ignored and almost all the oxygen vacancies are under the flatband condition, which consequently boost B1 band emission greatly (Fig. 3c). In contrast, B2 band (∼ 555 nm) compares favorably with B1 band for the sample whose surface is covered by small packed grains. Due to the small difference between the depletion width and actual grain size, most of V_O^+ convert to V_O^{++} states by trapping a hole from the grain surface [3]. Then, a radiative recombination of a conduction band photoexcited electron with a V_O^{++} center yields photons with energy of about 2 eV. It is just the reason why the visible emission band of the sample deposited at 60 pa had an obvious red-shift as shown in Fig. 3.

Recently, two representative mechanisms of the green emission have been presented. K. Vanheusden et al. [2] proposed the recombination of isolated V_O^+ center with photoexcited holes are responsible for the green emission and alternatively A. van Dijken et al. [11] identified the visible emission as a transition of a photo-generated electron from conduction band to a deep trap level. They are both reasonable, however, seem to conflict with one another. In fact, these two transitions are involved in the different grain regions on account of the changes in defect chemistry. The two discussed recombination models for the green emission of ZnO are derived in Fig. 5. In the bulk region, most oxygen vacancies are expected to be in V_O^+ states under flatband conditions. Consequently, the radiative transition of an electron from the V_O^+ level to the valance band is responsible for the 2.5 eV PL band. In contrast, in the depletion region, PL band around 2.2 eV is the contribution of the radiative recombination of a delocalized electron close to the conduction band with a deeply electron-trapped center (V_O^{++}). This model has shed some light on the transition mechanism of the green emission; however, further studies are still in progress to confirm the recombination centers and the detailed mechanism of the green emission.

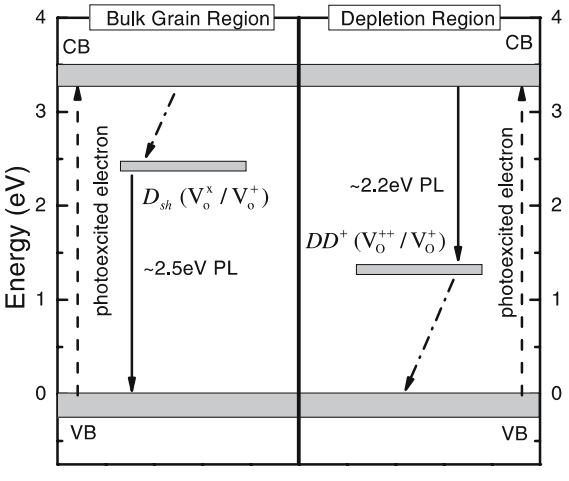

FIGURE 5 Sketches of the two radiative recombination processes under discussion for the green emission in ZnO

4 Conclusions

In summary, the present study shows the correlation between the green emission and the surface morphology of ZnO films in terms of the grain boundary defect model. With respect to the rough surface containing the large discrete island or structureless overgrowth based on the flat continuous layer, most of oxygen vacancies are of V_O^+ under flatband conditions, resulting in broad green emission around 2.5 eV. In contrast, when the surface covered by small close-packed grains which is greatly depleted, V_O^{++} are the dominant native defects, trapping a conduction band photoexcited electron and yielding photons with energy around 2.2 eV. These discussions have shed some light on the transition mechanism of ZnO for the green emission. In addition, high luminous efficiency of UV band corresponds to the smooth surface morphology with well-ordered grains, indicative of the reduction of the intrinsic defects and the improvement of the optical properties.

ACKNOWLEDGEMENTS Research supported by the special funds for Major State Basic Research Project of China (No.G001CB3095), National Natural Science Foundation of China (No.60276011 and No.60390073) and Project of High Technology Research & Development of China (No.2002AA311060)

REFERENCES

1 T. Aoki, Y. Hatanaka: Appl. Phys. Lett. **76**, 3257 (2000)
2 K. Vanheusden, W.L. Warren, C.H. Seager, D.R. Tallant, J.A. Voigt, B.E. Gnade: J. Appl. Phys. **79**, 7983 (1996)
3 A. van Dijken, E.A. Meulenkamp, D. Vanmaekelbergh, A. Meijerink: J. Lumin **87**, 454 (2000)
4 M. Liu, A.H. Kitai, P. Mascher: J. Lumin. **54**, 35 (1992)
5 B. Lin, Z. Fu, Y. Jia: Appl. Phys. Lett. **79**, 943 (2001)
6 S.A. Studenikin, N. Golego, M. Cocivera: J. Appl. Phys. **84**, 2287 (1998)
7 D. Hahn, R. Nink: Phys. Cond. Mater. **3**, 311 (1965)
8 A.F. Kohan, G. Ceder, D. Morgan: Phys. Rev. B **61**, 15 019 (2000)
9 D.C. Reynolds, D.C. Look, B. Jogai: Solid State Commun. **101**, 643 (1997)
10 F.H. Leiter, H.R. Alves, A. Hofstaetter: Phys. Status Solidi B **226**, R4–R5 (2001)
11 A. van Dijken, E.A. Meulenkamp, D. Vanmaekelbergh, A. Meijerink: J. Lumin. **90**, 123 (2000)
12 T.K. Gupta, W.D. Straub, M.S. Ramanachalam, J.P. Schaffer, A. Rohatgi: J. Appl. Phys. **66**, 6132 (1989)
13 D. Fernandez-Hevia, J. de Frutos, A.C. Caballero, J.F. Fernandez: Appl. Phys. Lett. **83**, 2692 (2003)
14 H.C. Ong, J.Y. Dai, G.T. Du: Appl. Phys. Lett. **81**, 277 (2002)
15 A. Iribarren R. Castro-Rodríguez, F. Caballero-Briones, J.L. Pena: Appl. Phys. Lett. **74**, 2957 (1999)
16 M. Godieski, E.M. Goldys, M.R. Phillips, R. Langer, A. Barski: Appl. Phys. Lett. **73**, 3686 (1998)
17 J.D. Ye, S.L. Gu, S.M. Zhu, T. Chen, F. Qin, L.Q. Hu, R. Zhang, Y. Shi, Y.D. Zheng: J. Crystal Growth **243**, 151 (2002)
18 D. Walton, T.N. Rhodin, W. Rollins: J. Chem. Phys. **38**, 2698 (1963)
19 M. Ohring: *The Materials Science of Thin Films* (London Academic Press, 1992), Chapts. 4 and 5
20 Y. Sun, J.B. Ketterson, G.K.L. Wong: Appl. Phys. Lett. **77**, 2322 (2000)
21 S.B. Zhang, S.H. Wei, A. Zunger: Phys. Rev. B **63**, 075 205 (2001)
22 C.H. Seager, T.G. Castner: J. Appl. Phys. **49**, 3879 (1978)
23 T. Tsurumi, S. Nishizawa, N. Ohashi, T. Ohgaki: Jpn. J. Appl. Phys. **38**, 3682 (1999)